

Ce and La single and double substitutional defects in yttrium aluminum garnet: First-principles study

Ana Belén Muñoz-García¹ and Luis Seijo^{1,2}

¹*Departamento de Química, Universidad Autónoma de Madrid, 28049 Madrid, Spain*

²*Instituto Universitario de Ciencia de Materiales Nicolás Cabrera,
Universidad Autónoma de Madrid, 28049 Madrid, Spain*

(Dated: January 17, 2011)

Abstract

The atomistic structure, energetics, and electronic structure of single substitutional Ce and La defects and double substitutional Ce-La defects in Ce,La-codoped yttrium aluminum garnet (YAG) $\text{Y}_3\text{Al}_5\text{O}_{12}$ have been studied by means of first-principles periodic boundary conditions density-functional theory calculations. Single substitution of Y by Ce or by La produces atomistic expansions around the impurities which are significantly smaller than the ionic radii mismatches and the overall lattice distortions are found to be confined within their second coordination spheres. In double substitutional defects, the impurities tend to be as close as possible. La-codoping Ce:YAG provokes an anisotropic expansion around Ce defects. The Ce impurity introduces $4f$ occupied states in the 5.0 eV computed gap of YAG, peaking 0.25 eV above the top of the valence band, and empty $4f$, $5d$, and $6s$ states starting at 3.8 eV in the gap and spreading over the conduction band. La-codoping produces very small effects on the electronic structure of Ce:YAG, the most visible one being the decrease of covalent bonding with one of the oxygen atoms, which shifts 0.05 Å away from Ce and gets 0.04 Å closer to La in the most stable Ce-La double substitutional defect.

PACS numbers: 71.55.-i, 61.72.-y, 61.72.J-

I. INTRODUCTION

Yttrium aluminum garnet $\text{Y}_3\text{Al}_5\text{O}_{12}$, or YAG, doped with Ce^{3+} is a blue-to-yellow converter phosphor used in white light solid-state lighting devices.^{1,2} A search for alternative phosphors, which present a higher efficiency and a better color-rendering index than Ce:YAG, is now on the way because of the growing interest in the development of highly efficient lamps for illumination.³⁻⁷

One of the lines followed in this search for new phosphors is codoping,³⁻⁵ because codopants are long ago known to be able to act as co-activators and as wavelength shifters. For instance, Tb^{3+} in Ce:YAG acts as a co-activator, enhancing the red spectral emission intensity and improving the color rendering index.³ Gd^{3+} and La^{3+} in Ce:YAG shift the yellow luminescence of Ce^{3+} to longer wavelengths (red shift),^{8,9} and, on the contrary, Ga^{3+} shifts it to shorter wavelengths (blue shift).^{1,8,9} These differential shifts formed the basis of an empirical rule which is in use,⁵ according to which substitutions of the dodecahedral Y^{3+} by larger ions red shift the Ce^{3+} emission and substitutions of the octahedral Al^{3+} by larger ions blue shift it.^{8,9} The lattice constants increase with both types of codopants, Gd^{3+} or La^{3+} on one side and Ga^{3+} on the other,⁹ which complicates the interpretations on the basis of increasing and decreasing crystal field splittings of the Ce^{3+} 5d shell,⁵ and makes it difficult to advance predictions. For instance, a compression of the local lattice surrounding the Ce^{3+} ions accompanying the expansion of the whole lattice was proposed in order to explain the red shift of the luminescence of Ce:YAG upon Gd^{3+} -codoping.¹⁰ Also in this line, codoping with Mg^{2+} and Si^{4+} red shifts the Ce emission⁸ and a similar red shift was anticipated by codoping with Mg^{2+} and Ti^{4+} , but a blue shift was found instead and the luminescence was severely quenched.⁵

Besides the manipulation of the luminescence of the Ce defects, codoping YAG with Ce and other rare earths finds other applications. For instance, Ce-codoping Nd:YAG was found to enhance near-infrared emission from the Nd defects two orders of magnitude.¹¹

Dopants may substitute for different atoms at several sites in YAG. Perfect garnets are usually described in terms of a 160 atom body-centered cubic unit cell (80 atom primitive cell), which contains eight formula units of $\text{A}_3\text{B}'_2\text{B}''_3\text{O}_{12}$, where A, B' and B'' are cations in different symmetry sites. In YAG, $\text{A} \equiv \text{Y}$ is eightfold coordinated in a distorted cubic D_2 local site, $\text{B}' \equiv \text{Al}$ is in an octahedral environment, and $\text{B}'' \equiv \text{Al}$ in a tetrahedral environment.

Idealized cubic YAG belongs to the $Ia\bar{3}d$ (230) space group, with Y in 24(c) sites, Al_{oct} in 16(a) sites, Al_{tet} in 24(d) sites, and the remaining 96 oxygen atoms in (h) sites, which depend on three x , y and z internal parameters.¹² Optically active Ce^{3+} impurities are known to substitute for Y^{3+} at D_2 (c) sites.^{1,9} These sites are also occupied by inactive Lu^{3+} , Gd^{3+} , and La^{3+} red shift inducing impurities^{5,9,13}, whereas Ga^{3+} and In^{3+} blue shift leading impurities substitute for Al^{3+} ions.⁵

A necessary condition in order to understand the factors that govern how the Ce:YAG luminescence depends on codoping and, ultimately, to be able to control the color of the Ce:YAG: phosphor via codoping, is to acquire a detailed knowledge of the local structures of the double or multiple substitutional defects at the atomistic level, as well as of their electronic structures. From this starting point, one can explore how the geometrical and electronic distortions induced by codoping change the manifold of excited states involved in the absorption and luminescent processes. This holds also for the mechanisms that control the energy transfer between Ce^{3+} and other rare earth codopants in materials like, i.e., Ce,Nd:YAG. However, experimental data on the detailed structures of the double defects created by codoping are not presently available. Obtaining such information by experimental techniques, like extended X-ray absorption fine-structure EXAFS, is very difficult and, as a matter of fact, not even the local structure of the single substitutional defect Ce_Y is known.

In this paper, we report the results of periodic-boundary-conditions DFT calculations of the local structures and the electronic structures of Ce_Y and La_Y single substitutional defects in YAG ($\text{Y}_{2.875}\text{Ce}_{0.125}\text{Al}_5\text{O}_{12}$ or Ce:YAG and $\text{Y}_{2.875}\text{La}_{0.125}\text{Al}_5\text{O}_{12}$ or La:YAG, respectively), and of the double substitutional $\text{Ce}_Y\text{-La}_Y$ defects resulting from Ce^{3+} and La^{3+} co-doping ($\text{Y}_{2.75}\text{Ce}_{0.125}\text{La}_{0.125}\text{Al}_5\text{O}_{12}$ or Ce,L a:YAG), all of them in their ground states. A few first-principles studies on perfect YAG and other garnets are available,^{14–19} as well as on some of its local defects, such as antisite defects²⁰ and Ce^{3+} single substitutional defects.²¹ Also, some pair-potential empirically parametrized atomistic simulations aimed at describing the energetics of formation of a number of defects such as impurities, interstitials and vacancies are also available.^{22–24} However, to the best of our knowledge, this is the first first-principles theoretical study in which the atomistic structures of double substitutional defects Ce,L a:YAG are calculated, as well as the associated electronic structures. Wave function based embedded-cluster calculations on the manifolds of excited states of the most stable double defects found in this paper, aimed at finding why La-codoping produces a red

shift of the Ce luminescence, have been reported elsewhere.²⁵

The methodological details are presented in Sec. II, the results on the materials with single substitutional defects, Ce:YAG and La:YAG, are shown and discussed in Sec. III A and those on the material with double substitutional defects, Ce,La:YAG, in Sec. III B. The conclusions are presented in Sec. IV.

II. DETAILS OF THE CALCULATIONS

All the structures of the single and double defects and their electronic structure analyses have been computed with the periodic boundary conditions self-consistent SIESTA method,^{26,27} using density functional theory^{28,29} (DFT) within the generalized gradient approximation (GGA) as formulated by Perdew, Burke, and Ernzerhof^{30,31} (PBE). Within this approach, the structures of all defects and the bonding properties are expected to be reliable. The details of the electronic structures related to Ce-4f and Ce-5d, particularly of their differences, should be taken with caution. We used norm-conserving pseudopotentials³² in the Kleinman-Bylander form.³³ For Y, Al, and O, we used those previously generated¹⁵ for the reference configurations Y($5s^2 4p^6 4d^1$), Al($3s^2 3p^1$), and O($2s^2 2p^4$) and for Ce and La the relativistic version³⁴ for the reference configurations Ce³⁺($5s^2 4p^6 4f^1$) and La³⁺($5s^2 4p^6$) generated in Ref. 25. Nonlinear partial-core corrections³⁵ and semicore states to account for large core-valence overlap have been used for Y and La. Atomic basis sets of double- ζ plus polarization quality have been used for all atoms: Y($5s 5s' 4p 4p' 5p 4d 4d'$), Al($3s 3s' 3p 3p' 3d$), O($2s 2s' 2p 2p' 3d$), Ce($5s 6s 6s' 5p 5p' 6p 5d 5d' 4f$), and La($5s 6s 6s' 5p 5p' 6p 5d 5d' 4f$). The basis sets of Y, Al, and O have been generated in Ref. 15 and those of Ce and La have been optimized in Ref. 25 in a similar manner, using the fictitious enthalpy method of Anglada *et al.*³⁶ in cubic CeAlO₃ and LaAlO₃ perovskites (with experimental lattice constants $a = 3.82$ Å and 3.74 Å respectively). The pseudopotentials and basis sets of Y, Al, and O have previously been used in calculations of perfect YAG, yttrium aluminum perovskite YAlO₃ (YAP), Al₂O₃, Y₂O₃, and antisite defects in YAG, with satisfactory results.^{15,20} Those of La have been checked in calculations of lattice constants and internal parameters of rhombohedral LaAlO₃ and cubic and hexagonal La₂O₃, with satisfactory results which are summarized in Table I. The charge density is projected on a uniform grid in real space, with an equivalent plane-wave cutoff of 380 Ry, in order to calculate the exchange-correlation and Hartree

matrix elements. Total energy calculations have been converged with respect to k -space integration; a k grid cutoff of 15.0 Bohr was used. All calculations are spin-polarized.

All geometry optimizations have been performed without imposing any symmetry restrictions in the position of all atoms in the unit cell, using a conjugate gradient method, with a force tolerance of 0.04 eV/Å. Starting geometries were generated from the computed atomistic structure of perfect YAG¹⁵ ($a=12.114$ Å, $x(\text{O})=-0.036$, $y(\text{O})=0.0519$ and $z(\text{O})=0.1491$, in good agreement with experiment,¹²⁾ upon substitution of Y atoms by Ce and/or La atoms to generate the single and double substitutional defects. We have explored the change in the volume of the unit cell produced by the substitutions by allowing the cell to breath after optimization of a defect. We obtained lattice constant increments of +0.11% in Ce:YAG²⁵ and +0.25% in La:YAG. These lattice expansions are small enough so as to consider negligible their effects on the local structures, which are the goal in this work, so that all the coordinates and energies in the paper correspond to $a=12.114$ Å.

III. RESULTS AND DISCUSSION

A. Ce and La single substitutional defects in YAG

1. Structure

The structural distortions around the single substitutional defects Ce_Y and La_Y corresponding to the doped materials $\text{Y}_{2.875}\text{Ce}_{0.125}\text{Al}_5\text{O}_{12}$ and $\text{Y}_{2.875}\text{La}_{0.125}\text{Al}_5\text{O}_{12}$ (one single substitutional defect per YAG unit cell) are summarized in Table II, where the displacements of the atoms in the first and second coordination shells are shown. No significant displacements have been found in atoms in the third shell and beyond, all of them being smaller than 0.005 Å.

Both Ce and La produce an expansion around them, as expected from the analysis of the ionic radii. The expansions of the first shells are, however, significantly smaller than the ionic radii mismatches: according to Shannon's ionic radii³⁷ of trivalent Y, Ce and La in 8-fold coordination (1.019, 1.143 and 1.16 Å respectively), the computed expansions of the first shell of oxygens are only one third and one fifth of the mismatch in Ce:YAG and one half in La:YAG. Having in mind the contrasted reliability of the method used here (both the SIESTA technical components and the PBE DFT functionals) and that a very similar

expansion has been found by Gracia *et al.*²¹ in wave function CASSCF/CASPT2 embedded cluster calculations on Ce:YAG, which are also reliable and fully independent of the present calculations, the above observation points out that ionic radii mismatches can only be taken as a qualitative indication, but not as a means to compute quantitative distortions, as it has previously been concluded out of embedded cluster structural calculations.^{38,39} The distance elongations created by La are larger and more homogeneous than those created by Ce (O1 and O2 expand almost the same in La:YAG, 3.3% and 3.1%, whereas O1 expand the double of O2 in Ce:YAG, 1.7% and 0.9%). However, although they are not large in any case, the lateral displacements are significantly bigger in La:YAG (0.02 Å for La-O2 and 0.03 Å for La-O1) than in Ce:YAG, where they are basically negligible. The overall distortion might well be described as a breathing expansion both in Ce:YAG and La:YAG, but specially in the first case. The structure of the first shell found in Ce:YAG is similar to that of a previous embedded cluster *ab initio* calculation²¹, where the Ce-O1 and Ce-O2 distances were 2.370 and 2.441 Å and the O1a-Ce-O1b angle was 72.4°.

The distortions of the second coordination shell are small but not negligible; the largest ones correspond to the Al_{tet}^a atoms, which belong to the AlO_4 moieties that share two oxygens with the MO_8 reference moiety (O1a and O1b). Observing the structures of these $\text{Al}_{tet}^a\text{O}_4$ moieties and their deformation when the Ce_Y and La_Y substitutional defects are formed is interesting for two reasons. One of them is that a popular description of YAG corresponds to a set of ionically bonded Y^{3+} , Al^{3+} , and $(\text{AlO}_4)^{5-}$ units. Another one is the observation that the chains $-\text{Y}-\text{AlO}_4-\text{Y}-\text{AlO}_4-$ are particularly tight in YAG [a $-\text{AlO}_4-\text{Y}-\text{AlO}_4-$ fragment of this chain along the x axis is shown in Fig. 1]. This observation, which was not reported before to the best of our knowledge, is shown by the facts that $d(\text{M}-\text{Al}_{tet}^a)$ is significantly shorter than $d(\text{M}-\text{Al}_{tet}^b)$ [Al_{tet}^b belongs to a AlO_4 moiety that shares one oxygen atom only with MO_8] and the angles $\alpha(\text{O1a}-\text{Al}_{tet}^a-\text{O1b})$ and $\alpha(\text{O}_{ext}^a-\text{Al}_{tet}^a-\text{O}_{ext}^b)$ are significantly smaller than the tetrahedral angles (109.5°) as a consequence of the stress imposed on the $\text{Al}_{tet}^a\text{O}_4$ tetrahedron by one Y bonded to O1a and O1b in one side and another Y bonded to O_{ext}^a and O_{ext}^b in the opposite side of the chain. Also note that $d(\text{Y}-\text{O1})$, which is an element of one of these chains, is significantly shorter than $d(\text{Y}-\text{O2})$, which is not.

The $\text{Al}_{tet}^a\text{O}_4$ moiety shows some flexibility upon Y substitution by Ce and La. The changes of the O-Al-O angles make them closer to the tetrahedral ones, more in La:YAG than in Ce:YAG, releasing part of the angular stress and allowing the aluminum atom to have more

sp^3 character. The $\text{Al}_{tet}^a\text{-O1}$ and $\text{Al}_{tet}^a\text{-O}_{ext}$ distances are: 1.788-1.788 Å, 1.792-1.783 Å, and 1.779-1.776 Å, in YAG, Ce:YAG, and La:YAG, respectively. Altogether, distances and angles show that Ce pushes O1a and O1b opening the O1a- Al_{tet}^a -O1b angle but elongating the O1-Al bonds slightly, also slightly displacing Al_{tet}^a , whereas the larger distortion induced by La pushes O1a and O1b harder, both opening the O1a- Al_{tet}^a -O1b angle and shrinking the O1-Al bonds so much that Al_{tet}^a is significantly displaced and the $\text{O}_{ext}^a\text{-Al}_{tet}^a\text{-O}_{ext}^b$ angle is also significantly opened.

The overall distortion created by La_Y in YAG is larger than the one created by Ce_Y . This is also shown by the defect stress energies, E_{stress} , which are 323 meV/defect (31.2 kJ/mol) for La:YAG and 125 meV/defect (12.1 kJ/mol) for Ce:YAG. E_{stress} is defined as the difference between the energies per unit cell of the substituted material with the structure of the host (YAG) and with the fully relaxed structure. Only local strains are considered here. The fact that distortions beyond the second coordination shell are negligible supports neglecting global strains at the considered dopant concentrations. Higher concentrations would presumably demand them.

The energies for replacing an Y^{3+} ion by a Ce^{3+} and a La^{3+} ion are 0.113 eV (11 kJ/mol) and 3.710 eV (358 kJ/mol) respectively, which refer to the processes $8 \text{Y}_3\text{Al}_5\text{O}_{12} + \text{M}_{vacuum}^{3+} \rightarrow 8 \text{Y}_{2.875}\text{M}_{0.125}\text{Al}_5\text{O}_{12} + \text{Y}_{vacuum}^{3+}$ with M being Ce and La, respectively. These defect formation energies are small, the Ce one being smaller than that of La. Both of them are much smaller than the equivalent ones of Ca-substitutional and Mg-substitutional defects, which amount around 20 eV per defect as calculated in empirical shell-model simulations in Ref. 24. The solution enthalpy of La_2O_3 in YAG that corresponds to the process $8 \text{Y}_3\text{Al}_5\text{O}_{12} + \frac{1}{2} \text{La}_2\text{O}_3 \rightarrow 8 \text{Y}_{2.875}\text{La}_{0.125}\text{Al}_5\text{O}_{12} + \frac{1}{2} \text{Y}_2\text{O}_3$, can be calculated out of the energies per unit cell of the four solids; our result is 3.635 eV (351 kJ/mol).

2. Electronic structure

The band structures of La:YAG and Ce:YAG do not show significant differences with that of YAG (Ref. 15) and they are not shown here. Total densities of states (DOS) and projected densities of states (PDOS) of these materials are shown in Fig. 2 for La:YAG and in Figs. 3 and 4 for Ce:YAG. The La impurity introduces $5p$ occupied states around -17 and -12.5 eV ($5s$ peaks at -29 eV) and $4f$, $5d$, and $6s$ empty states spread above 5 eV, with a

prominent $4f$ peak at 6 eV that coincides with the Y empty states at the bottom of the conduction band of the YAG host. Y, Al, and O states do not suffer significant distortions with respect to YAG. The Ce impurity introduces $5p$ occupied states between -18 and -16 eV and between -14 and -12 eV, and new states in the host gap: one isolated localized $4f$ state with single occupancy 0.25 eV above the top of the valence band and empty states of $4f$, $5d$ and $6s$ character start appearing at 3.8 eV in the gap of YAG and show two prominent $4f$ peaks at 4.25 and 4.75 eV (the calculated band gap of YAG is 5.0 eV¹⁵). The difference between occupied and empty states of the Ce impurity is 2.63 eV. This value is not to be compared with the lowest $4f \rightarrow 4f$ transitions in Ce:YAG, which are in fact much less energetic,²¹ because changes in the occupancies of the unfilled shells will make the DOS and PDOS to change very much. The same is true for all $4f \rightarrow 4f$, $4f \rightarrow 5d$, and $4f \rightarrow 6s$ transitions, which should not be assigned to the series of peaks in Fig. 4 (center) starting at 4.25 eV, 4.75 eV, 6.25 eV, and further on.

It is interesting to observe the effect of the Ce impurity on the PDOS of its first neighbor oxygens, as shown in the bottom of Fig. 4. It reveals that, whereas the O2 PDOS remains almost intact with respect to O in YAG, the O1 PDOS is significantly altered in the energy region of Ce $4f$ occupied orbitals. The O1 PDOS gain in the 0.2-0.8 eV region indicates a significant interaction between the atomic orbitals of the O1 oxygens and the Ce $4f$ orbitals that is not shown by the O2 oxygens. The O1 oxygens are the ones that make the $(-Y-AlO_4-Y-AlO_4)_n$ tight chains in YAG.

B. Ce and La co-doped YAG

1. Structure

Seven Ce_Y-La_Y double substitutional defects of the material $Y_{2.75}Ce_{0.125}La_{0.125}Al_5O_{12}$ have been studied, all of them corresponding to one Ce_Y and one La_Y per YAG unit cell. The list spans all double substitutions of this kind in which the distance between the Ce_Y and La_Y sites which are in the same YAG unit cell are, before relaxation, smaller than or equal to the distance between this Ce_Y site and another translation equivalent La_Y site lying in a different unit cell. In Table III we show the corresponding Ce_Y-La_Y distances and the relative energies of the seven double defects, together with the reference Y-Y distances

and the distances between impurities in different unit cells. The energy differences between the defects are not large, but two of them are clearly more stable than the other: they correspond to the smallest Ce-La distances. So, according to these calculations, the Ce and La impurities tend to be as close as possible in Ce,La:YAG.

The structures of the two most stable double defects (defect 1 and defect 2 in Table III) are shown in Fig. 5 and detailed in Table IV.

In defect 1, which is the most stable of all, there are significant distortions around the Ce_Y and La_Y sites with respect to the single defects. The overall effect of La on the coordination shell of Ce is an expansion (of 0.010 Å on average). On average, the four oxygens of type O1, which are the nearest to Ce, experience an expansion of 0.019 Å, whereas the remaining four oxygens, of type O2, which are the most distant to Ce, maintain their distance (average expansion of 0.001 Å). On the other hand, the overall effect of Ce on the coordination shell of La is a contraction (of 0.006 Å on average). In this case, the four nearest oxygens of type O1 maintain their average distance to La whereas the more distant O2 oxygens experience an average contraction of 0.013 Å. Individually, the eight oxygens around Ce and the eight around La suffer very different displacements from their reference positions, resulting in eight different Ce-O distances and eight different La-O distances, with the D_2 local site symmetries around Ce_Y in Ce:YAG and around La_Y in La:YAG being completely lost in Ce,La:YAG. The largest displacement is experienced by O_B , which is one of the two bridging oxygens between the CeO_8 and LaO_8 moieties; it increases its distance to Ce by 0.054 Å and gets closer to La by 0.040 Å. However, the other bridging oxygen, O_A , does not experience an important displacement. The displacement of O_B may be observed together with the change in the Ce-La distance and the displacements of other oxygens: Ce-La suffers an elongation of 0.01 Å with respect to Ce-Y in Ce:YAG, which indicates that Ce and La push each other and they shift away in order to relax the stress energy; Ce gets closer to O_2 and La to O_c and to O_d , all of them around 0.01 Å, as a result of Ce and La pushing each other away (these are all oxygens opposite to the respective codopant), and the remaining oxygens either stay or shift away a little bit from the impurities in order to accommodate the previous atomic rearrangements.

It is interesting to see that the Ce-La distance is very similar to the Y-La distance in La:YAG whereas it is significantly longer than the Ce-Y distance in Ce:YAG. This means that the relative positions of the cations is dominated by La, which pushes away Ce and Y

in an equal amount. Then, the effect of La-codoping on Ce in defect 1 can be described as an anisotropic pushing that forces Ce to weaken its bonding with the bridging oxygen O_B ; this oxygen gets away from Ce and closer to La and the remaining oxygens slightly relocate their positions, both around Ce and around La.

In defect 2, where Ce and La locate at around 5.7 Å from each other, the distortions around La with respect to La:YAG are negligible and the Ce-La distance is virtually equal to the Y-La distance in La:YAG, although 0.01 Å shorter than Ce-Y in Ce:YAG. This supports the idea developed after the analysis of defect 1 that La controls the relative cation location (Ce-La in Ce,La:YAG and Y-La in La:YAG). As in defect 1, the anisotropic effect of La on the Ce site alters the bonding between Ce and the oxygens, which in this case makes significantly longer Ce- O_3 and Ce- O_5 and shorter O_4 bonds, with an overall expansion of the first coordination shell of oxygens of 0.009 Å (on average, the closest oxygens of type O_1 expand 0.005 Å and the most distant O_2 oxygens expand 0.012 Å). However, the feedback effect of these rearrangements on the LaO_8 moiety are negligible in this case because no bridging oxygens are present and the surroundings of La are basically untouched with respect to La:YAG.

As we have just seen, the overall effect of La on the first coordination shell of Ce_Y for the two most stable configurations of the double substitutional defects Ce_Y-La_Y is a local expansion. This result does not support a recent hypothesis made in order to explain the red shift experienced by the $5d \rightarrow 4f$ luminescence of Ce:YAG upon Gd-codoping, according to which there is a local lattice compression around the Ce^{3+} ions when Gd^{3+} ions are added to replace Y^{3+} in the YAG lattice, in spite of the fact that the lattice constant expands upon Gd-codoping Ce:YAG.¹⁰ Although Gd^{3+} and La^{3+} are different, both of them produce red shift in Ce:YAG and they are expected to do it for a common reason.⁸ A wave function based first-principles calculation of the type embedded cluster CASSCF/CASPT2 based on the present atomistic structures²⁵ shows they are consistent with a $4f \rightarrow 5d$ red shift induced by the La-codoping.

The stress energies of the double defects 1 and 2 are 0.465 eV/defect (44.8 kJ/mol) and 0.460 eV/defect (44.4 kJ/mol) respectively. These are the energy lowerings when all atoms relax their positions after Ce substitutes one Y and La substitutes another Y. These values are only slightly larger than the sum of the stress energies of the individual defects Ce_Y (0.125 eV/defect, 12.1 kJ/mol) and La_Y (0.323 eV/defect, 31.2 kJ/mol): 0.448 eV/defect

or 43.3 kJ/mol. The binding energy between two relaxed single defects to form one relaxed double defect results to be 0.059 eV/defect (5.7 kJ/mol) for defect 1 and 0.062 eV/defect (6.0 kJ/mol) for defect 2. Subtracting from these values the above relaxation energy differences (0.017 eV/defect and 0.012 eV/defect for defects 1 and 2) gives the binding energy between the stressed (unrelaxed) single Ce_Y and La_Y defects to form the stressed double Ce_Y - La_Y defects: 0.042 eV/defect (4.2 kJ/mol) for defect 1 and 0.050 eV/defect (4.9 kJ/mol) for defect 2.

Relaxing the lattice constant with the presence of the double defects 1 and 2 gives small expansions of 0.32% and 0.31% respectively. This, together with the short extension of the distortions, suggest that the interactions between defects in adjacent unit cells are negligible and, as in the case of single Ce and La defects, justifies neglecting global strains at the dopant concentrations under consideration.

2. *Electronic structure*

In Fig. 6 we show the total DOS of Ce,L a:YAG corresponding to the structure of defect 1, together with its PDOS of Ce, La, Y, Al, and O atoms and the orbital decomposition of the Ce PDOS. The equivalent results in the case of defect 2 are very similar to these. The total DOS of Ce,L a:YAG resembles very much those of the parent materials Ce:YAG and La:YAG , because the contribution of Y, Al, and O are very similar in the three materials. Some features to remark are, first, that Ce,L a:YAG shows the peaks between -14 and -12 eV that correspond to the superposition of basically independent $\text{La-5}p$ and $\text{Ce-5}p$ states, and, second, that the structure of the $\text{O-2}p$ valence band is remarkably closer to the same band in Ce:YAG than in La:YAG ; this is the consequence of a mixing between $4f$ and $\text{O-2}p$ states, which is small but significant in Ce and negligible in La.

It is interesting to observe in the bottom of Fig. 6 the PDOS of O_B in Ce,L a:YAG (Fig. 5), which is the oxygen in the CeO_8 moiety that suffers the biggest effect upon La-codoping. When we compare it with its PDOS in Ce:YAG we can see how the higher energy contribution is slightly shifted to lower energies. This is a consequence of the bonding between Ce and O_B diminishing, since this is the contribution of the states with highest mixing between $\text{Ce-4}f$ and $\text{O-2}p$. The 0.25 eV shift to lower energies of the Ce states is also experienced by its innermost $5s$ and $5p$ orbitals, which indicates that this is not a bonding

effect, but the consequence of the change of the electrostatic field on Ce due to its off-center displacement forced by the presence of La.

As we mentioned before in the case of Ce:YAG, we cannot identify peaks in the DOS lying above the Fermi level of Ce,La:YAG with the observed $4f \rightarrow 5d$ blue absorptions of the Ce defects and, as a consequence, we cannot use these results to calculate the red-shift experienced by these transitions upon La-codoping. In this respect, wave function based embedded-cluster calculations on this materials can take advantage of the present structural studies and be used to make reliable predictions on the effects of La-codoping on the shift of the $4f \rightarrow 5d$ electronic transitions. Such kind of calculations are presently being performed in our lab and they will be the subject of a future report.

IV. CONCLUSIONS

First-principles periodic boundary conditions density-functional theory calculations have been performed on the atomistic structure and electronic structure of Ce-doped, La-doped, and Ce,La-codoped yttrium aluminum garnet (YAG) $\text{Y}_3\text{Al}_5\text{O}_{12}$. In the Ce_Y and La_Y single substitutional defects, the impurities produce expansions around them which are significantly smaller than the ionic radii mismatches and the overall lattice distortions are found to be confined within their second coordination spheres. In Ce_Y - La_Y double substitutional defects, the impurities tend to be as close as possible. The effect of La-codoping on the local structure around Ce defects in Ce:YAG is found to be an anisotropic expansion in overall, in contrast with a recent proposition of local lattice compression.

The analysis of the electronic structure of Ce:YAG reveals that the Ce impurity introduces $4f$ occupied states in the 5.0 eV computed gap of YAG, peaking 0.25 eV above the top of the valence band, and empty $4f$, $5d$, and $6s$ states starting at 3.8 eV in the gap and spreading over the conduction band. A strong covalent interaction is found between Ce and the four nearest oxygens of its eightfold coordination shell which is significantly larger than with the four more distant oxygens. La-codoping produces very small effects on the electronic structure of Ce:YAG, the most visible one being the decrease of covalent bonding with one of the oxygen atoms, which shifts 0.05 Å away from Ce and gets 0.04 Å closer to La.

Acknowledgments

We are grateful to Professor Z. Barandiarán, Universidad Autónoma de Madrid, for discussions and a careful reading of the manuscript. This work was partly supported by a grant from Ministerio de Ciencia e Innovación, Spain (Dirección General de Programas y Transferencia de Conocimiento MAT2008-05379/MAT). A.B.M.-G. acknowledges a contract of the program Personal Investigador en Formación (Comunidad de Madrid).

-
- ¹ Blasse, G.; Bril, A. *J. Chem. Phys.* **1967**, *47*, 5139.
- ² Jüstel, T.; Nikol, H.; Ronda, C. *Angew. Chem., Int. Ed.* **1998**, *37*, 3084.
- ³ Jang, H. S.; Im, W. B.; Lee, D. C.; Jeon, D. Y.; Kim, S. S. *J. Lumin.* **2007**, *126*, 371.
- ⁴ Lin, Y. S.; Liu, R. S.; Cheng, B.-M. *J. Electrochem. Soc.* **2005**, *152*, J41.
- ⁵ Pan, Y.; Wu, M.; Su, Q. *J. Phys. Chem. Solids* **2004**, *65*, 845.
- ⁶ Tanner, P. A.; Fu, L.; Ning, L.; Cheng, B.-M.; Brik, M. G. *J. Phys.: Condens. Matter* **2007**, *19*, 216213.
- ⁷ Zorenko, Y.; Gorbenko, V.; Konstankevych, I.; Voloshinovskii, A.; Stryganyuk, G.; Mikhailin, V.; Kolobanov, V.; Spassky, D. *J. Lumin.* **2005**, *114*, 85.
- ⁸ Robertson, J. M.; van Tol, M. W.; Smits, W. H.; Heynen, J. P. H. *Philips J. Res.* **1981**, *36*, 15.
- ⁹ Tien, T. Y.; Gibbons, E. F.; DeLosh, R. G.; Zacmanidis, P. J.; Smith, D. E.; Stadler, H. L. *J. Electrochem. Soc.* **1973**, *120*, 278.
- ¹⁰ Pan, Y. X.; Wang, W.; Liu, G. K.; Skanthakumar, S.; Rosenberg, R. A.; Guo, X. Z.; Li, K. K. *J. Alloys Compd.* **2009**, *488*, 638.
- ¹¹ Meng, J. X.; Li, J. Q.; Shi, Z. P.; Cheah, K. W. *Appl. Phys. Lett.* **2008**, *93*, 221908.
- ¹² Euler, F.; Bruce, J. A. *Acta Crystallogr.* **1965**, *19*, 971.
- ¹³ Holloway, W. W.; Kestigian, M. J. *Opt. Soc. Am.* **1969**, *59*, 60.
- ¹⁴ Freeman, C. L.; Allan, N. L.; van Westrenen, W. *Phys. Rev. B* **2006**, *74*, 134203.
- ¹⁵ Muñoz-García, A. B.; Anglada, E.; Seijo, L. *Int. J. Quantum Chem.* **2009**, *109*, 1991.
- ¹⁶ Pari, G.; Mookerjee, A.; Bhattacharya, A. K. *Physica B* **2005**, *365*, 163.
- ¹⁷ Pascale, F.; Zicovich-Wilson, C. M.; Orlando, R.; Roetti, C.; Ugliengo, P.; Dovesi, R. *J. Phys. Chem. B* **2005**, *109*, 6146.

- ¹⁸ Shelyapina, M. G.; Kasperovich, V. S.; Wolfers, P. *J. Phys. Chem. Solids* **2006**, *67*, 720.
- ¹⁹ Xu, Y.-N.; Ching, W. Y. *Phys. Rev. B* **1999**, *59*, 10530.
- ²⁰ Muñoz-García, A. B.; Artacho, E.; Seijo, L. *Phys. Rev. B* **2009**, *80*, 014105.
- ²¹ Gracia, J.; Seijo, L.; Barandiarán, Z.; Curulla, D.; Niemansverdriet, H.; van Gennip, W. *J. Lumin.* **2008**, *128*, 1248.
- ²² Kuklja, M. *J. Phys.: Condens. Matter* **2000**, *12*, 2953.
- ²³ Milanese, C.; Buscaglia, V.; Maglia, F.; Anselmi-Tamburini, U. *Chem. Mater.* **2004**, *16*, 1232.
- ²⁴ Schuh, L.; Metselaar, R.; Catlow, C. R. A. *J. Europ. Ceram. Soc.* **1991**, *7*, 67.
- ²⁵ Muñoz-García, A. B.; Pascual, J. L.; Barandiarán, Z.; Seijo, L. *Phys. Rev. B* **2010**, *82*, 064114.
- ²⁶ Ordejón, P.; Artacho, E.; Soler, J. M. *Phys. Rev. B* **1996**, *53*, R10441.
- ²⁷ Soler, J. M.; Artacho, E.; Gale, J. D.; García, A.; Junquera, J.; Ordejón, P.; Sánchez-Portal, D. *J. Phys.: Condens. Matter* **2002**, *14*, 2745.
- ²⁸ Hohenberg, P.; Kohn, W. *Phys. Rev. B* **1964**, *136*, B864.
- ²⁹ Kohn, W.; Sham, L. J. *Phys. Rev.* **1965**, *140*, A1133.
- ³⁰ Perdew, J. P.; Burke, K.; Ernzerhof, M. *Phys. Rev. Lett.* **1996**, *77*, 3865.
- ³¹ Perdew, J. P.; Burke, K.; Ernzerhof, M. *Phys. Rev. Lett.* **1997**, *78*, 1396.
- ³² Troullier, N.; Martins, J. L. *Phys. Rev. B* **1991**, *43*, 1993–2006.
- ³³ Kleinman, L.; Bylander, D. M. *Phys. Rev. Lett.* **1982**, *48*, 1425–1428.
- ³⁴ Bachelet, G. B.; Hamann, D. R.; Schlüter, M. *Phys. Rev. B* **1982**, *26*, 4199.
- ³⁵ Louie, S. G.; Froyen, S.; Cohen, M. L. *Phys. Rev. B* **1982**, *26*, 1738.
- ³⁶ Anglada, E.; Soler, J. M.; Junquera, J.; Artacho, E. *Phys. Rev. B* **2002**, *66*, 205101.
- ³⁷ Shannon, R. D. *Acta Crystallogr. A* **1976**, *32*, 751.
- ³⁸ Seijo, L.; Barandiarán, Z. *Int. J. Quantum Chem.* **1996**, *60*, 617.
- ³⁹ Seijo, L.; Barandiarán, Z. In *Computational Chemistry: Reviews of Current Trends*; Leszczyński, J., Ed.; World Scientific: Singapore, 1999; Vol. 4, pp 55–152.
- ⁴⁰ Wu, B.; Zinkevich, M.; Aldinger, F.; Zhang, W. *J. Phys. Chem. Solids* **2007**, *68*, 570.
- ⁴¹ S. A. Hayward, F. D. Morrison, S. A. T. Redfern, E. K. H. Salje,; ; Scott, J. F.; Knight, K. S.; Tarantino, S.; Glazer, A. M.; Shuvaeva, V.; Daniel, P.; Zhang, M.; Carpenter, M. A. *Phys. Rev. B* **2005**, *72*, 054110.
- ⁴² Hirosaki, N.; Ogata, S.; Kocer, C. *J. Alloys Compd.* **2003**, *351*, 31.
- ⁴³ Wyckoff, R. W. G. *Crystal Structures*; Wiley, 1968.

TABLE I: Lattice constants and internal parameters of LaAlO_3 ($R\bar{3}c$, 167), cubic La_2O_3 ($Ia\bar{3}$, 206), and hexagonal La_2O_3 ($P\bar{3}m1$, 164).

LaAlO_3				
	LDA (Ref. 40)	GGA (Ref. 40)	This work	Experiment (Ref. 41)
a (Å)	5.306	5.417	5.375	5.36977
c (Å)	12.931	13.189	12.942	13.0860
x_O	0.533	0.541	0.523	0.5288
La_2O_3 (cubic)				
	LDA (Ref. 42)		This work	Experiment (Ref. 43)
a (Å)	11.392		11.388	11.360
x_O	0.3892		0.3796	0.385
y_O	0.1482		0.1492	0.145
z_O	0.3787		0.3782	0.380
x_{La}	0.9709		0.9712	0.965
La_2O_3 (hexagonal)				
	LDA (Ref. 42)		This work	Experiment (Ref. 43)
a (Å)	3.936		3.888	3.933
c (Å)	6.166		6.128	6.129
z_O	0.6454		0.655	0.630
z_{La}	0.2469		0.231	0.235

TABLE II: Distortions in the first and second coordination shells around Ce_Y and La_Y substitutional defects with respect to pure YAG. For each atom, the following parameters are given: δr_{\parallel} and δr_{\perp} , which stand for its radial displacement along the M-atom axis and its perpendicular displacement with respect to that axis, and Θ , which is the angle between the radial displacement and the displacement vectors of the atom. α stands for angles between three atoms. Atom labels correspond to Figure 1. Distances in Å, angles in degree.

		YAG M=Y	Ce:YAG M=Ce	La:YAG M=La
First coordination shell				
M-O1	d(M-O1)	2.333	2.373 (+1.7%)	2.410 (+3.3%)
	δr_{\parallel}	-	0.041	0.076
	δr_{\perp}	-	0.004	0.027
	Θ	-	6.5	19.6
M-O2	d(M-O2)	2.446	2.468 (+0.9%)	2.522 (+3.1%)
	δr_{\parallel}	-	0.023	0.076
	δr_{\perp}	-	0.006	0.019
	Θ	-	12.0	14.2
$\alpha(\text{O1a-M-O1b})$		72.2	72.1	70.9
$\alpha(\text{O2a-M-O2b})$		108.2	107.9	107.5
$\alpha(\text{O2b-M-O2c})$		73.6	73.7	74.1
Second coordination shell				
M- Al_{tet}^a	d(M- Al_{tet}^a)	3.028	3.046 (+0.6%)	3.063 (+1.1%)
	δr_{\parallel}	-	0.012	0.034
	δr_{\perp}	-	0.000	0.000
	Θ	-	0.0	0.0
$\alpha(\text{O1a-Al}_{tet}^a\text{-O1b})$		100.5	102.3	103.6
$\alpha(\text{O}_{ext}^a\text{-Al}_{tet}^a\text{-O}_{ext}^b)$		100.5	101.1	102.1
$\alpha(\text{O}_{ext}^a\text{-Al}_{tet}^a\text{-O1a})$		114.1	113.4	112.8
M- Al_{oct}	d(M- Al_{oct})	3.386	3.401 (+0.4%)	3.410 (+0.7%)
	δr_{\parallel}	-	0.013	0.023
	δr_{\perp}	-	0.005	0.005
	Θ	-	20.4	12.7
M-Y	d(M-Y)	3.709	3.718 (+0.2%)	3.726 (+0.5%)
	δr_{\parallel}	-	0.007	0.017
	δr_{\perp}	-	0.003	0.004
	Θ	-	25.2	13.9
M- Al_{tet}^b	d(M- Al_{tet}^b)	3.709	3.718 (+0.2%)	3.727 (+0.5%)
	δr_{\parallel}	-	0.009	0.020
	δr_{\perp}	-	0.003	0.003
	Θ	-	20.2	7.8

TABLE III: Distances between Ce_Y and La_Y defects in the same unit cell of Ce,La:YAG , in Å. The values of the shortest inter-cell Ce_Y - La_Y distances are also given, together with the number of such pairs. Relative defect energies with respect to the most stable, in meV and kJ/mol (in parenthesis).

	YAG $d(\text{Y-Y})$	$d(\text{Ce}_Y\text{-La}_Y)$ intra-cell	Ce,La:YAG $d(\text{Ce}_Y\text{-La}_Y)$ inter-cell	ΔE
defect 1	3.709	3.728	9.314 x 1	0 (0)
defect 2	5.666	5.654	8.290 x 1	3 (0.3)
defect 3	6.057	6.058	6.058 x 1	48 (4.6)
defect 4	6.772	6.781	6.783 x 1	35 (3.4)
defect 5	7.103	7.117	9.329 x 1, 9.334 x 1	12 (1.2)
defect 6	8.566	8.573	8.559 x 1, 8.563 x 1, 8.569 x 1	20 (1.9)
defect 7	10.491	10.494	10.484-10.499 x 7	21 (2.1)

TABLE IV: Selected interatomic distances in the two most stable $\text{Ce}_Y\text{-La}_Y$ disubstitutional defects in Ce,L a:YAG . The distances between Ce and La in the two defects are given, together with reference distances between atoms occupying the same sites in La:YAG , Ce:YAG , and YAG . Distances between the substitutional atoms (Ce, La) and the oxygen atoms in their first coordination shell are also given. Oxygen labels correspond to Figure 5. Type 1 and type 2 oxygens refer to O1 and O2 types of coordination oxygens in Table II. Distance changes with respect to single substitutional defects in Ce:YAG and La:YAG are given in parentheses. Distances in Å, angles in degree.

	YAG	Ce:YAG	La:YAG	Ce,La:YAG
	d(Y-Y)	d(Ce-Y)	d(Y-La)	d(Ce-La)
defect 1	3.709	3.718	3.726	3.728
defect 2	5.666	5.668	5.651	5.654
defect 1	d(Ce-O)		d(La-O)	
	Oxygens of type 1			
	O_B	2.427 (+0.054)	O_A	2.417 (+0.007)
	O_1	2.385 (+0.012)	O_a	2.412 (+0.002)
	O_4	2.374 (+0.001)	O_c	2.399 (-0.011)
	O_5	2.383 (+0.010)	O_e	2.416 (+0.006)
	Oxygens of type 2			
	O_A	2.470 (+0.002)	O_B	2.482 (-0.040)
	O_2	2.460 (-0.008)	O_b	2.522 (0.000)
	O_3	2.513 (0.000)	O_d	2.510 (-0.012)
	O_6	2.477 (+0.009)	O_f	2.524 (+0.002)
defect 2	d(Ce-O)		d(La-O)	
	Oxygens of type 1			
	O_1	2.373 (0.000)	O_b	2.409 (-0.001)
	O_2	2.366 (-0.007)	O_c	2.411 (+0.001)
	O_5	2.407 (+0.034)	O_f	2.409 (-0.001)
	O_6	2.367 (-0.006)	O_g	2.411 (+0.001)
	Oxygens of type 2			
	O_3	2.512 (+0.044)	O_a	2.524 (+0.002)
	O_4	2.453 (-0.015)	O_d	2.524 (+0.002)
	O_7	2.475 (+0.007)	O_e	2.522 (0.000)
	O_8	2.476 (+0.008)	O_h	2.518 (-0.004)

FIG. 1: Partial representation of the first, second and third coordination shells around a Y site in YAG. The Y site is labelled M. The eight oxygens in the first shell are labelled O1 and O2: a couple of O1 oxygens belong to a common AlO_4 moiety whereas each of the O2 oxygens belongs to a different AlO_4 moiety. The second shell is made of two Al_{tet}^a aluminum atoms in the vertical axis, which belong to the AlO_4 moiety that shares two oxygens with M, plus four Al_{tet}^b aluminiums in tetrahedral sites, four Al_{oct} aluminiums in octahedral sites, and four Y cations; the Al_{tet}^b are linked to the O2 oxygens, and the Al_{oct} and Y cations are linked to one O1 and one O2 oxygens. The third shell is made of all the remaining oxygens in the first coordination shells of the mentioned cations. Note that the horizontal and vertical axes, as well as the axis perpendicular to them, are C_2 symmetry axes.

FIG. 2: PDOS of La, Y, Al, and O atoms in La:YAG, and total DOS of La:YAG and YAG. The Fermi level is indicated with a dashed line.

FIG. 3: PDOS of Ce (α and β spins), Y, Al, and O atoms in Ce:YAG, and total DOS of Ce:YAG and YAG. The Fermi level is indicated with a dashed line.

FIG. 4: Above: Orbital decomposition of the Ce α PDOS in Ce:YAG. Center: zoom over the gap zone of the Ce α and β PDOS. Below: PDOS for the first neighbor oxygen atoms of the Ce impurity in Ce:YAG O1 and O2 (Fig. 1), together with that of O in YAG and Ce in Ce:YAG for comparison. The peak at 0.25 eV corresponds to one isolated localized state with single occupancy; DOS and PDOS have been plotted by broadening eigenvalues with a gaussian peak width of 0.2eV.

FIG. 5: Representation of the two most stable Ce_Y-La_Y double substitutional defects. Above: defect 1. Below: defect 2.

FIG. 6: PDOS of Ce(α and β spins), La, Y, Al, and O atoms, total DOS, and orbital decomposition of the Ce α PDOS for the most stable double substitutional defect (defect 1) in Ce,L:YAG. The peak right above the top of the valence band corresponds to one isolated localized state with single occupancy. The Fermi level is indicated with a dashed line.

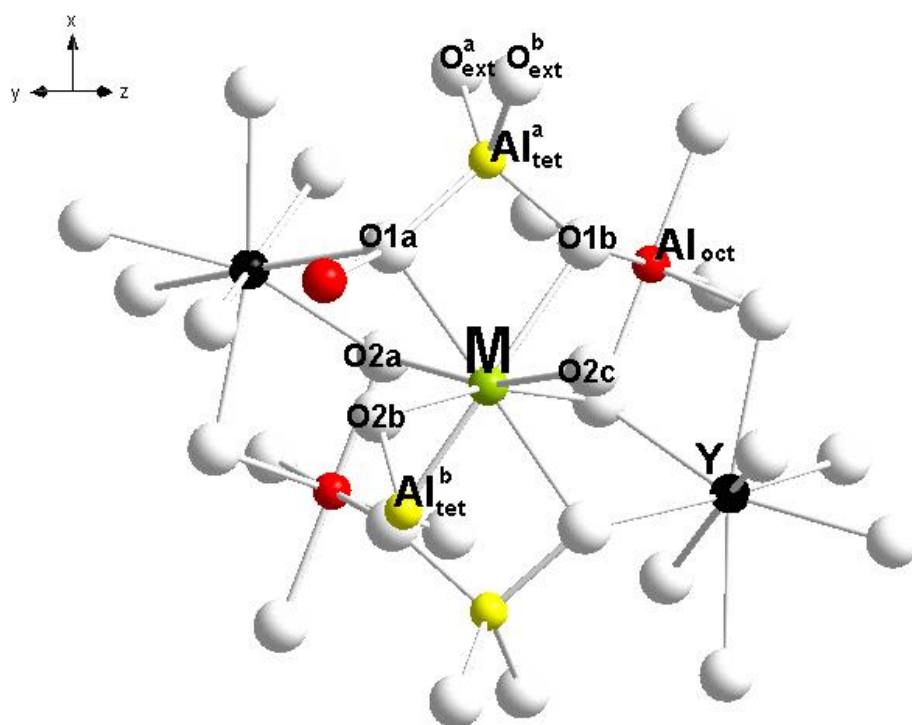


Figure 1 Muñoz-García and Seijo

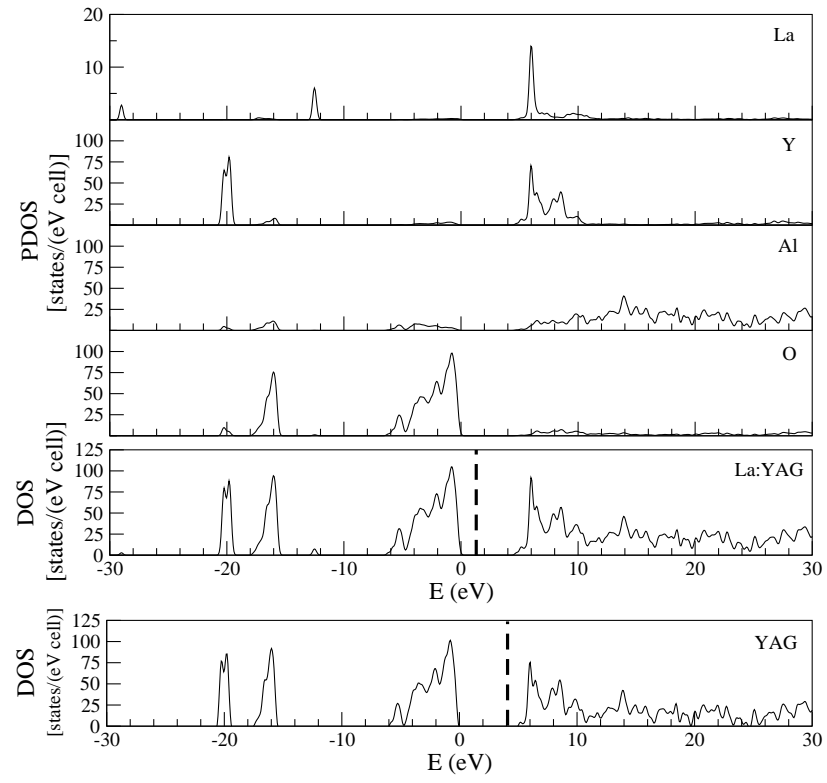


Figure 2 Muñoz-García and Seijo

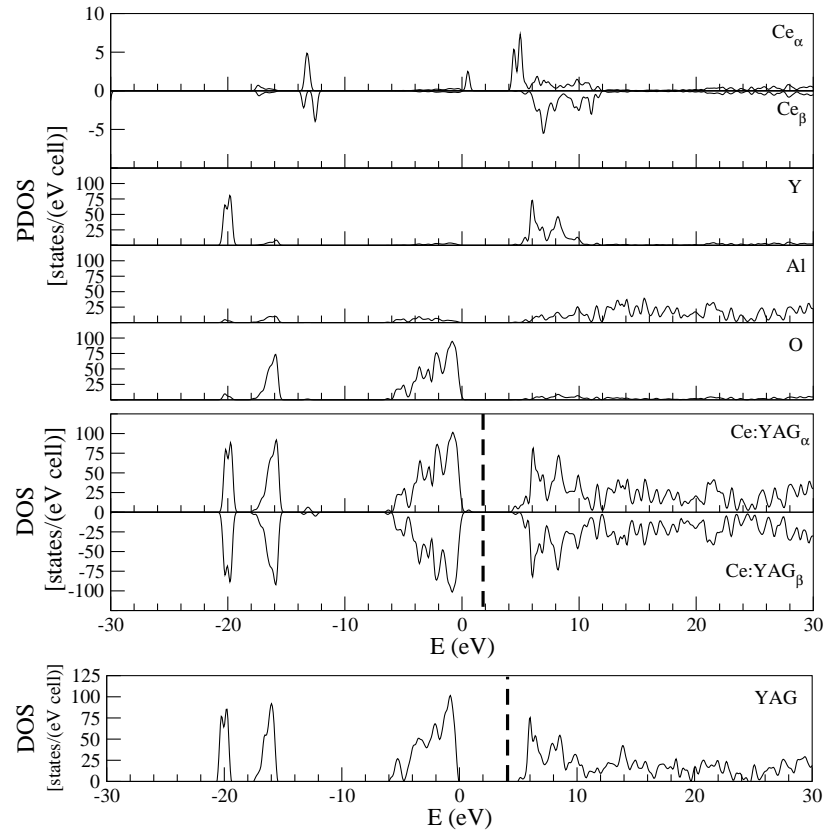


Figure 3 Muñoz-García and Seijo

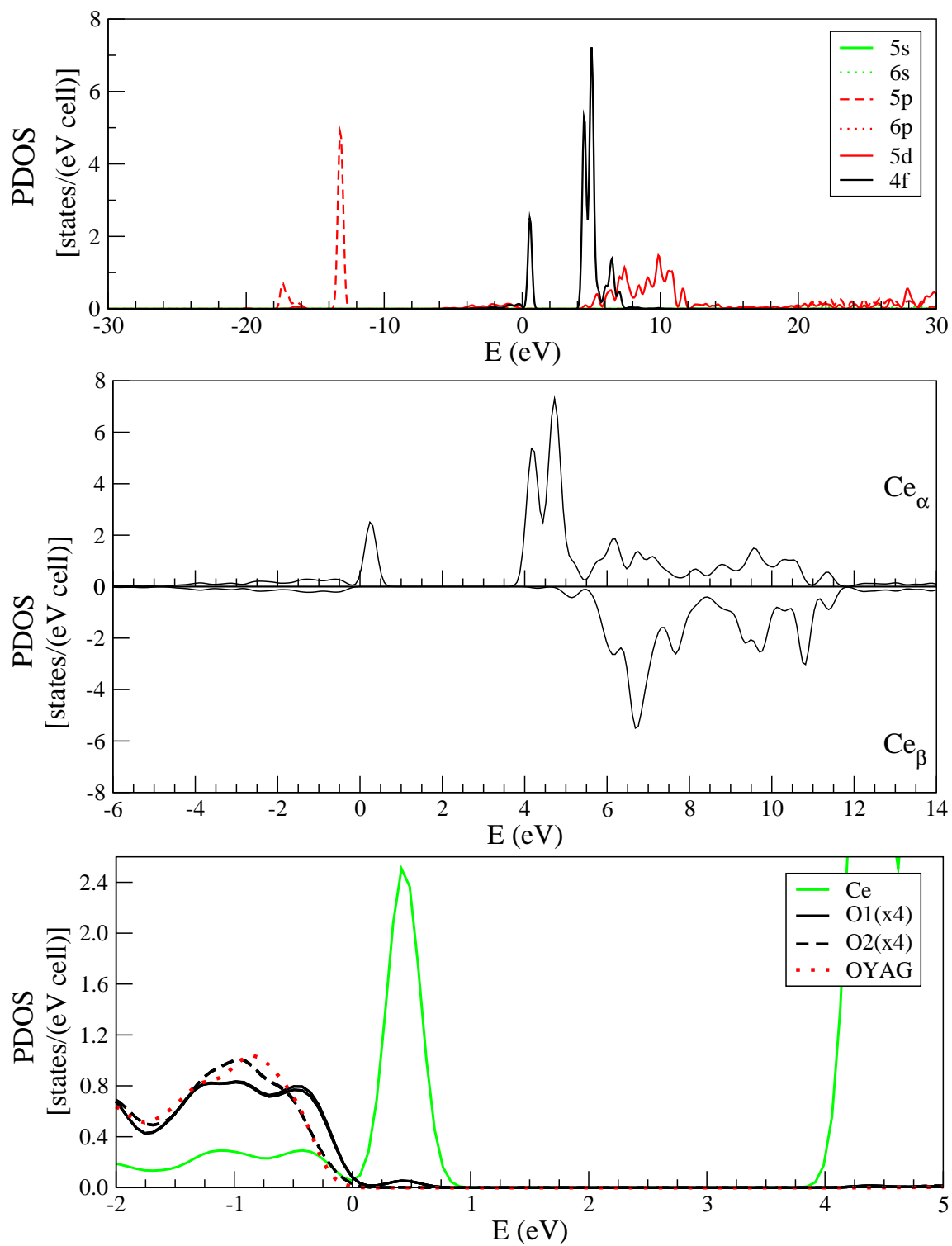


Figure 4 Muñoz-García and Seijo

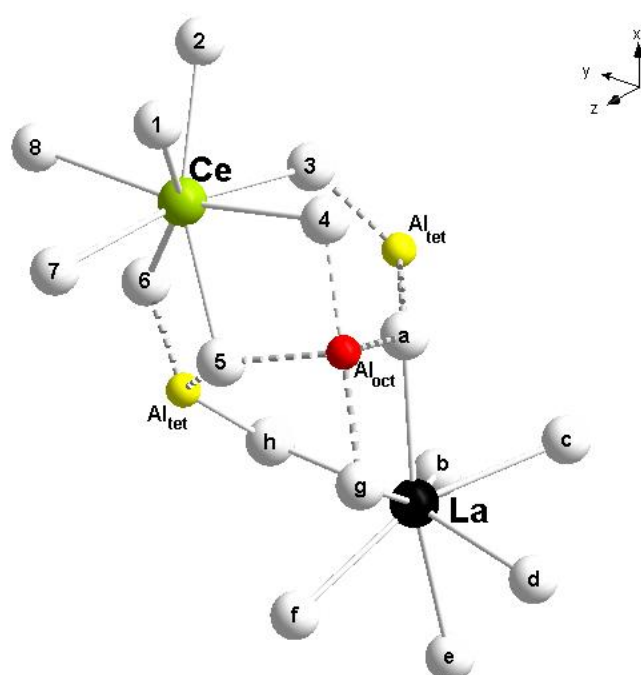
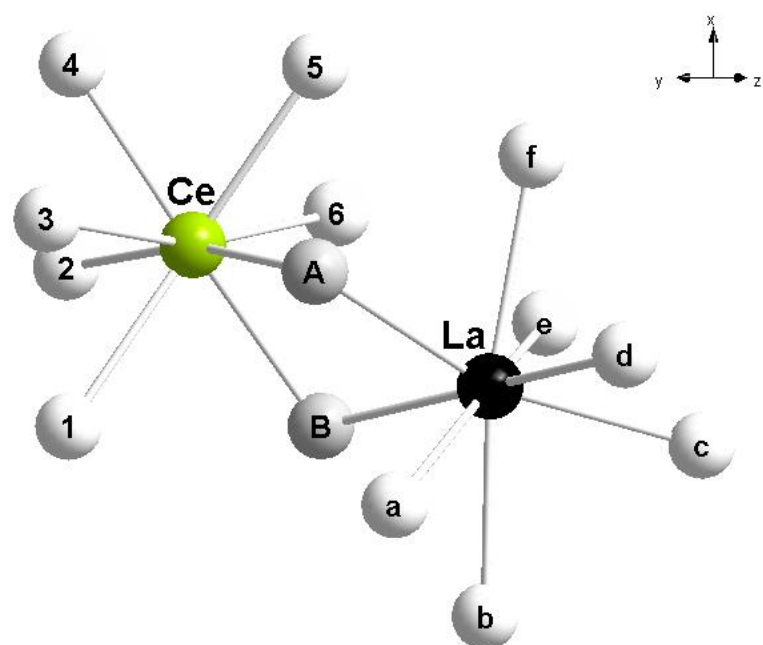


Figure 5 Muñoz-García and Seijo

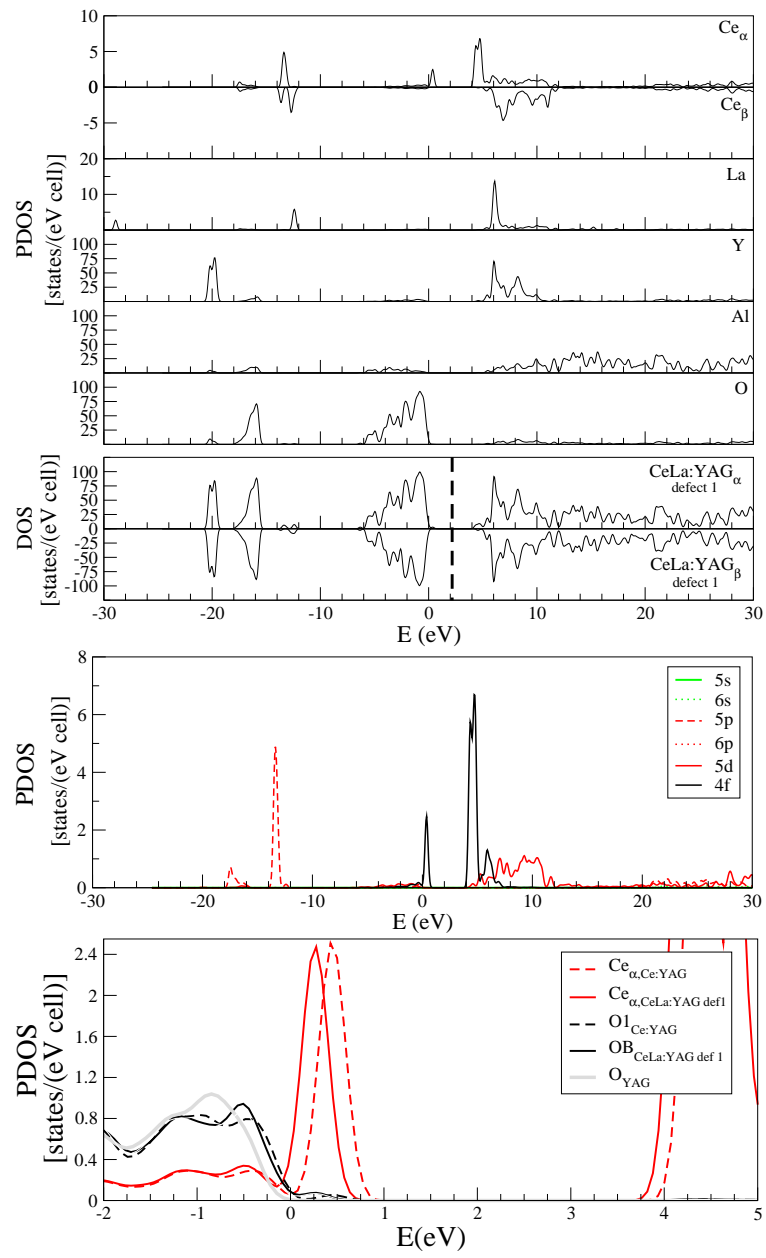
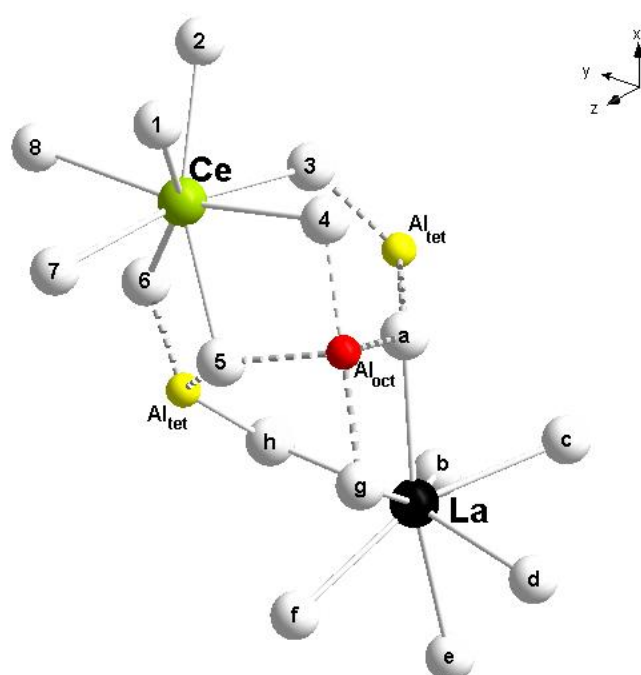
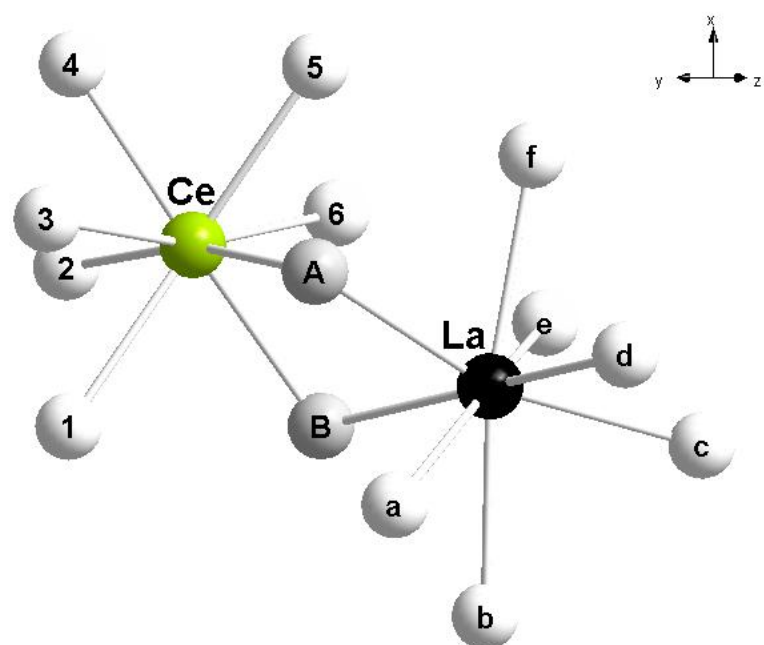


Figure 6 Muñoz-García and Seijo



TOC graphics